Turkish Journal of Electrical Engineering & Computer Sciences

http://journals.tubitak.gov.tr/elektrik/

Research Article

Turk J Elec Eng & Comp Sci
(2016) 24: 3609 – 3620

doi:10.3906/elk-1406-161

Process time and MPPT performance analysis of CF, LUT, and ANN control methods for a PMSG-based wind energy generation system

Abdulhakim KARAKAYA*, Ercüment KARAKAŞ
Department of Energy Systems Engineering, Technology Faculty, Kocaeli University, Kocaeli, Turkey

Received: 23.06.2014 • **Accepted/Published Online:** 20.05.2015 • **Final Version:** 20.06.2016

Abstract: Due to environmental issues such as global warming and the greenhouse effect, there is a growing interest in renewable sources of energy. Wind energy, which is the most important of these energy sources, can potentially meet a portion of the global energy demand. Numerous studies are being conducted worldwide to determine how the maximum level of power can be obtained from wind energy. In these studies, there is a particular interest in permanent magnet synchronous generators (PMSGs). This is because PMSGs exhibit a good performance within a wide range wind speeds and can be driven directly. In this study, the maximum power point tracking (MPPT) of a PMSG has been carried out by using a prototype built in a laboratory environment. The simulation model has been realized by utilizing MATLAB/Simulink and implemented by using dSPACE. MPPT has been performed by employing such control algorithms as an artificial neural network, a look-up table, and curve fitting in order to carry out comparative performance analyses of these control algorithms. Controllers were analyzed through comparisons between their MPPT and process performance. Based on our analysis results, we were able to identify controllers that were better in terms of power tracking and process performance.

Key words: Maximum power point tracking, permanent magnet synchronous generator, artificial neural network, look-up table, curve fitting, wind energy

1. Introduction

The continuous increase in energy demand, energy costs, and environmental awareness in the present-day world has led to a greater need to produce and use energies that are both renewable and clean. For this reason, technologies that produce alternative and renewable energy have been the subject of considerable emphasis and interest in recent years around the world. The wind generator is one such technology on which numerous studies have been conducted. These studies also indicate an increasing interest in permanent magnet synchronous generators (PMSGs).

Based on an evaluation of previous studies performed with the artificial neural network (ANN), look-up table (LUT), and curve-fitting (CF) controllers [1–10], it is possible to see that Hui et al. [1] performed the maximum power point tracking (MPPT) of a low-power PMSG by utilizing the results of a simulation in which wind speed was estimated with an ANN controller. The control method they proposed was then applied to a variable-speed cage induction machine wind generation system. In addition, they also found that the ANN performed better than the CF and LUT controllers during MPPT. However, such a study was not performed. Eskander [2], on the other hand, proposed an ANN model that allows MPPT for a wind energy conversion

*Correspondence: abdkarakaya@hotmail.com

system (WECS) and then evaluated the simulation results obtained with this model. Bharanikumar and Kumar [3] designed a WECS that uses a PMSG and employed a matrix converter to control the output voltage and frequency of this system. This WECS and a matrix convertor were modeled using PSIM, and the obtained results were further controlled through experiments. Lin [4] controlled the output values of a three-phased PMSG used in a wind turbine emulator by employing a recurrent neural network and examined the results obtained when applying this system. Demirtaş and Şerefoğlu [5] performed MPPT and determined the best design for a wind turbine control system by using a dsPIC-controlled DC/DC boost converter. Based on their experimental results, they determined that the designed mode provided 35% better efficiency than the normal mode. Meharrar et al. [6], on the other hand, proposed an ANFIS controller structure in order to determine the maximum power point of a variable-speed wind generator and tested this controller structure with a simulation. They then compared the simulation results for the ANFIS and fuzzy logic controllers. Zhang et al. [7] used the LUT algorithm to estimate solar radiation; based on the method they proposed, they were able to significantly develop the downward surface shortwave radiation estimations for regions with periodic meteorological conditions and complex terrain by using LUT controllers. Employing the LUT method, Benammar et al. [8] estimated angles based on the sinus and cosine signals generated by the resolver and sinusoidal encoder. They also examined the performance of this method by comparing the simulation results with the experimental results. Pradhan and Subudhi [9] performed an autotuning-based MPPT for a photovoltaic system. To determine the maximum power point, they made use of the polynomial CF method. This method was modeled on MATLAB/Simulink and the simulation results of the method were compared with its experimental results. Garrigos et al. [10] performed the MPPT of a photovoltaic module by using a microcontroller; they then used the CF method for verification purposes. Garrigos et al. emphasized that this method is simple, practical, and low-cost for real-time applications. However, it is possible to see that numerous other MPPT control algorithms have been used in studies [11–22]. In the present study, the MPPT of a PMSG was performed with an experimental set-up established in a laboratory environment and by using the ANN, LUT, and CF controllers. During the applications performed with the MATLAB/Simulink model, the MPPT and process performances of the ANN, LUT, and CF controllers were tested based on the desired and experimental results. MPPT was performed at reference speeds determined based on wind speed. The process performance of the controllers was tested and compared using a computer.

2. Wind turbine generator system

The equation for the amount of power obtained from wind turbines is shown in Eq. (1).

$$P_m = C_p P_w = C_p \frac{1}{2} \rho A V_w^3 \tag{1}$$

In Eq. (1), P_m is mechanical power (W), P_w is wind power (W), ρ is air density (kg/m^3), A is swept area (m^2), C_p is the power coefficient of the wind turbine, and V_w is wind speed (m/s).

In Eq. (1), if the wind speed, air density, and swept area are stable and fixed, the output power of the turbine will be a function of the power coefficient. The wind turbine characteristic $C_{p-\lambda}$ curve, where λ is tip-speed ratio, is given in Eq. (2).

$$\lambda = \frac{\omega_{rm} R}{V_w} \tag{2}$$

Here, R is the radius of the blades and ω_{rm} is the rotational speed of the wind turbine shaft. Figure 1 shows the $C_{p-\lambda}$ curve of the wind turbine designed for the PMSG that was used within the context of this study. As shown in Figure 1, at λ_{opt}, the C_p value is equal to Cpmax, which represents the optimum value. When Eq. (1) and Figure 1 are evaluated, it can be clearly seen that the C_p value must be at Cpmax for maximum power transfer. Figure 2 shows the relationship between the wind speed and the shaft speed and output power. In Figure 2, the maximum power curve (P_{max}) for the PMSG was obtained for different wind speeds. As an example, the P_m (W) – n (rpm) change was provided for four different wind speeds (V_{w1}, V_{w2}, V_{w3}, and V_{w4}).

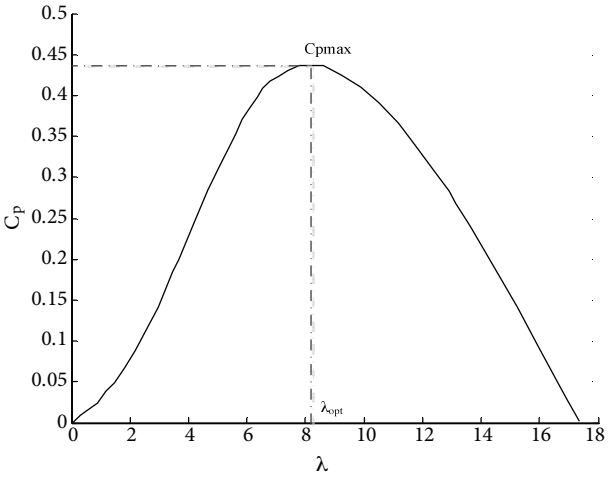

Figure 1. Tip-speed ratio of wind turbine.

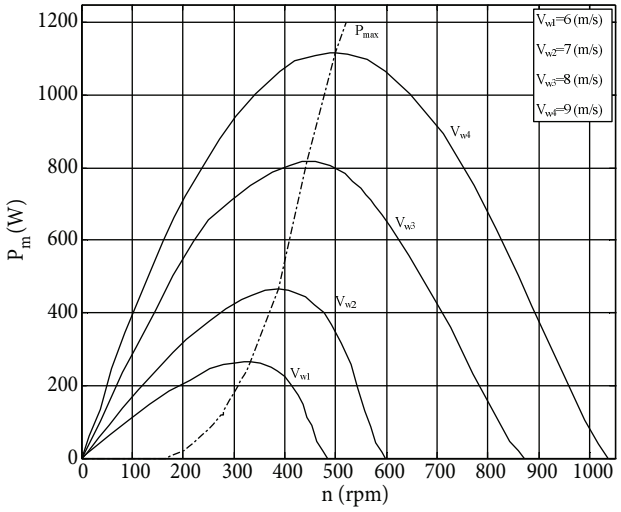

Figure 2. Variation in P_m, n, and P_{max} values according to different wind speeds.

3. Mathematical model of PMSG

For the PMSG, the mathematical equations for the reference frame of the d-q axes synchronous rotor are expressed as follows [23,24]: the vector representation of the transformation is presented in Figure 3, while Figure 4 shows the d-q equivalent circuit of the PMSG. In Figure 3, θ_r represents the angle of the q axis with the stator phase winding, while ω_r represents the electrical rotor speed (the synchronous speed). The d-q voltage equations for the stator windings are shown in Eqs. (3) and (4) below.

$$v_d = -r_s i_d + \frac{d(\lambda_d)}{dt} - \omega_r \lambda_q \tag{3}$$

$$v_q = -r_s i_q + \frac{d(\lambda_q)}{dt} + \omega_r \lambda_d \tag{4}$$

In Eqs. (3) and (4), v_d and v_q represent the d-q axis stator voltage, i_d and i_q represent the d-q axis stator currents, r_s represents the stator resistance per phase, and λ_d and λ_q represent the d-q axis currents. The λ_d and λ_q equalities in Eqs. (3) and (4) are similar to those in Eqs. (5) and (6).

$$\lambda_d = -L_d i_d + \lambda_m \tag{5}$$

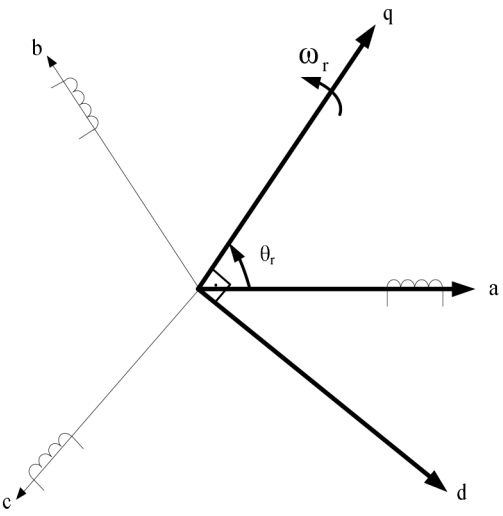

Figure 3. The abc to d-q frame transformation.

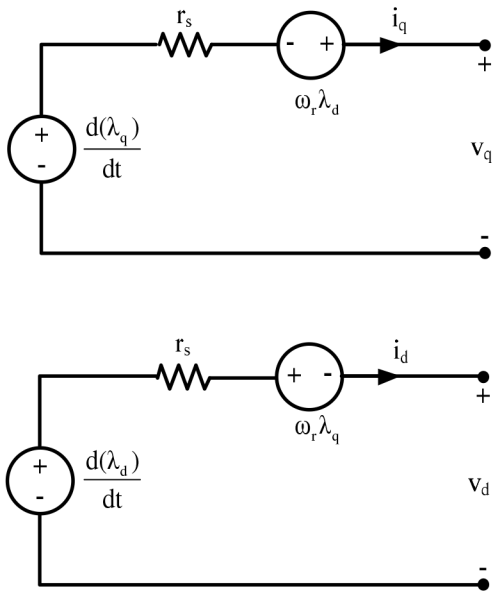

Figure 4. The d-q equivalent circuit of the PMSG.

$$\lambda_q = -L_q i_q \tag{6}$$

In Eqs. (5) and (6), L_d and L_q represent the d-q axis inductance values, while λ_m represents the excitation current formed by the magnetic materials on the stator coils.

The equations for the electromagnetic torque, the electrical speed, and the mechanical speed of the PMSG are given in Eqs. (7), (8), and (9), respectively.

$$T_e = \frac{3}{2}\frac{P}{2}\left[\left(L_d - L_q\right) i_d i_q + \lambda_m i_q\right] \tag{7}$$

$$\omega_r = \frac{P}{2}\omega_{rm} \tag{8}$$

$$\omega_{rm} = \frac{2\pi n}{60} \tag{9}$$

Here, ω_r shows the electrical speed of the rotor (rad/s), T_e is electromagnetic torque (Nm), n is rotor shaft speed (rpm), and ω_{rm} is the mechanical speed of the rotor (rad/s).

4. Experimental set-up

Figure 5 provides the block diagram for the proposed experimental set-up. As shown in this block diagram, the DC motor and PMSG are coupled with one another, and the PMSG is driven by a DC motor. The DC motor is used in place of the wind turbine whose characteristics are summarized in Section 2. The voltage obtained from the PMSG was rectified with a thyristor convertor. By filtering the rectified voltage, an ohmic load (R_L) was supplied. As the aim of this study was to carry out the performance analysis of the controllers, a previously designed thyristor rectifier was used. For this reason, it is possible to use semiconductor materials such as IGBT or MOSFET in the thyristor drive section.

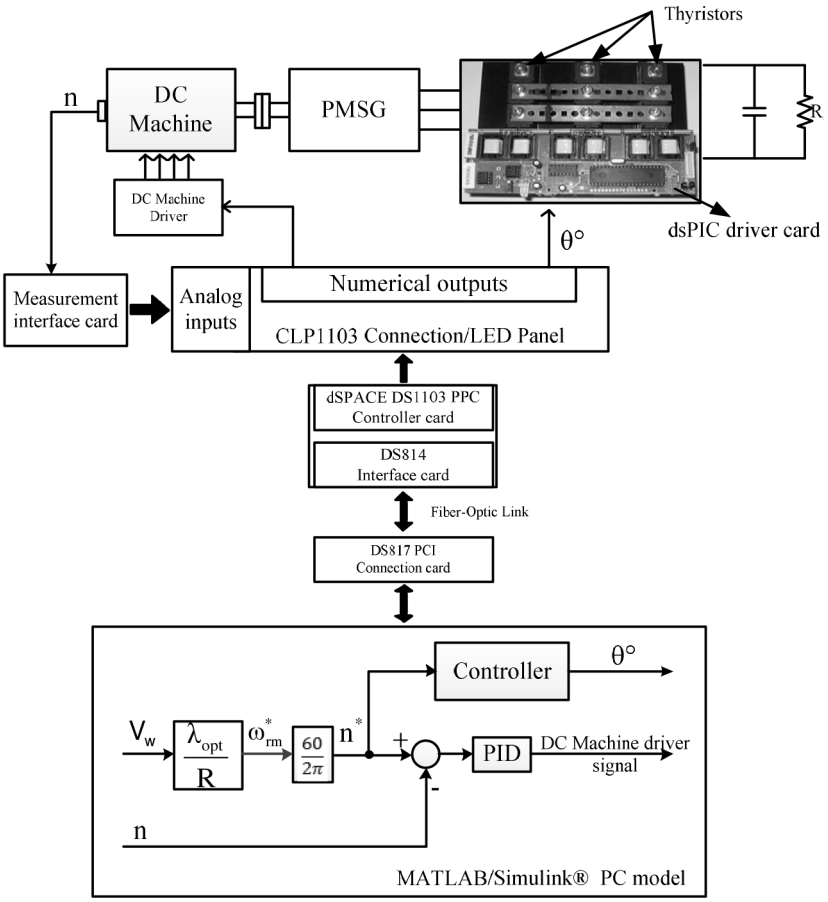

Figure 5. The block diagram of the proposed system.

For the control of the dsPIC drive card shown in Figure 5, the MATLAB/Simulink/Real-Time Workshop produced by the company MathWorks was used, along with the Real-Time Interface (RTI) and ControlDesk software developed by dSPACE. The RTI and ControlDesk software provided by dSPACE were used for performing applications and collecting real-time data. RTI is software used for applying Simulink models on real-time hardware, without any programming being necessary. The ControlDesk software of dSPACE allowed the transfer, evaluation, analysis, and recording of the experimental results in a computer environment.

Applications were performed using the ANN, LUT, and CF controllers at the controller block of the MATLAB/Simulink PC model shown in Figure 5. The rotor speed (n^*) was obtained by using the reference speed (ω^*_{rm}) determined based on the wind speed (V_w). The controllers determined the thyristor switching angles based on the n^* value. DC motor speed is controlled by a PID controller according to reference speed and the PMSG shaft was driven according to wind speed. Figure 6 shows the block diagram that describes how dsPIC identifies zero transition points of the phases.

5. Maximum power tracking

To obtain maximum power from the PMSG, the C_p value shown in Eq. (1) must be at its maximum value. For this reason, the tip-speed ratio shown in Figure 1 must be maintained at its optimum level ($\lambda_{opt} = 8.14$). In addition, by using Eq. (10) based on the P_{max}-n change in the PMSG in Figure 2, it is possible to perform

MPPT at reference speed values (ω^*_{rm}) obtained based on wind speeds. The switching angles of the thyristors were obtained by the controllers based on the reference speeds, which were determined according to wind speed. The PMSG was operated at maximum power points (P_{max}) based on the optimum switching angles that were obtained. Figure 7 shows the block diagram for the MPPT algorithm. Maximum power values with respect to wind and shaft speeds are shown in Table 1.

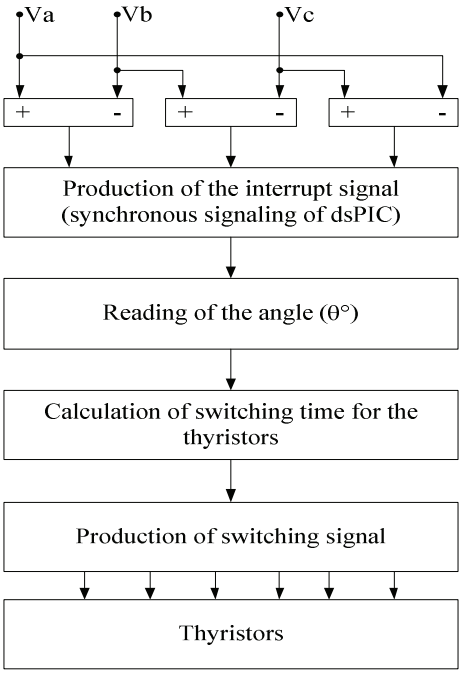

Figure 6. Block diagram on the production of dsPIC switching signals.

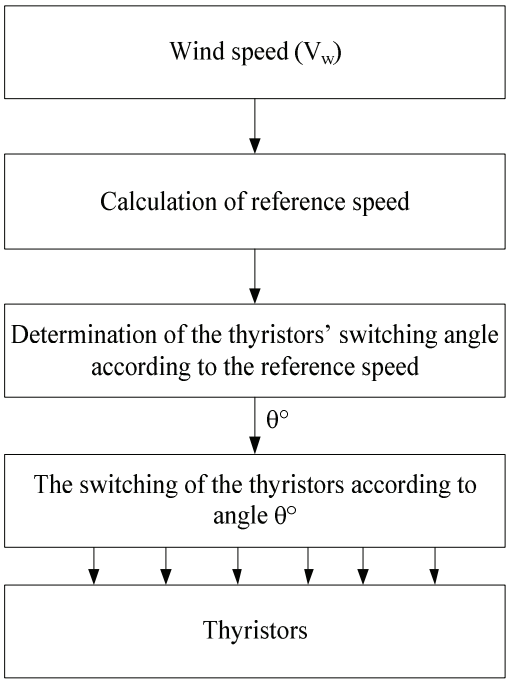

Figure 7. The block diagram for the MPPT algorithm.

Table 1. Maximum power values according to wind and shaft speeds.

Data used for training the controllers			Data used for testing the controllers		
V_w (m/s)	n* (rpm)	Obtained P_{max} (W)	V_w (m/s)	n* (rpm)	Obtained P_{max} (W)
5.41	300	144.764	4.95	275	123.569
6.31	350	213.015	5.85	325	183.465
7.21	400	286.476	6.74	375	251.615
8.1	450	367.452	7.64	425	323.582
9	500	446.215	8.54	475	406.235
9.9	550	543.417	9.46	525	494.885
10.79	600	634.813	10.36	575	597.307
11.69	650	711.727	11.26	625	673.529
12.59	700	788.174	12.15	675	749.789
13.52	750	873.214	13.05	725	829.598

$$\omega^*_{rm} = \frac{V_w \lambda_{opt}}{R} \tag{10}$$

In Table 1, the ω^*_{rm} speed values (rad/s) obtained with Eq. (10) based on the wind speed were converted into

an n* (rpm) value by using Eq. (9). The maximum power values obtained by following this conversion are also shown in Table 1. In conclusion, maximum power transfer will be achieved if the PMSG is driven by the DC motor at reference speeds, and if the thyristors are switched to optimum angles depending on the wind speed.

6. MPPT controllers

LUT, CF, and ANN controllers were separately used in the controller block shown in Figure 5 in order to perform MPPT. The MPPT algorithms of these controllers are provided below. The recommended training scheme for the ANN is shown in Figure 8. The reference speed (n*) obtained according to the wind speed, and the thyristor switching angle values corresponding to these speeds, are provided in Table 2. More data could have been used for ANN training; however, as all controllers were tested under similar conditions, the number of sample data shown in Table 2 was deemed sufficient. For each speed, the thyristor switching angle was determined by trial and error method. With this method, the thyristor switching angles were modified for each reference speed of the PMSG such that the maximum power would be obtained from the DC busbar. Training was performed using the ANN model shown in Figure 9, and by using different sample speeds in the model. The first hidden layer of this network had three tan-sigmoid neurons, while the second hidden layer had eleven. The output layer, on the other hand, had one linear neuron. For the input network parameter, the generator speed, and the output network parameter, the thyristor switching angle was θ° . Training was performed in 98 cycles by using the 11 input-output patterns shown in Table 2. The MATLAB/Simulink block of the ANN that has completed its trainings is shown in Figure 10.

Table 2. Data used in training and testing.

Data used in training		Data used in testing	
n* (rpm)	θ°	n* (rpm)	θ°
0	0	275	65
300	61	325	48
350	42	375	34
400	30	425	25
450	19	475	15
500	11	525	8
550	4	575	2
600	2	625	2
650	2	675	2
700	2	725	2
750	2		

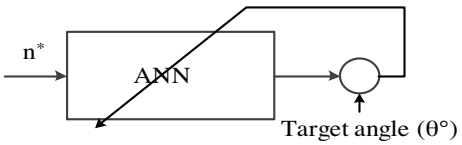

Figure 8. Proposed training scheme for ANN-based thyristor switching angle estimation.

The LUT block shown in Figure 10 was obtained from the MATLAB/Simulink library, and the training data in Table 2 were entered into this block. The LUT block performed the linear interpolation of the entered data. In addition, the CF block shown in Figure 10 is the "Fcn" block from the MATLAB/Simulink library. Eq. (11), which was obtained through the CF method, was entered into this block. The coefficients of the fifth degree polynomial equation that were obtained are given below.

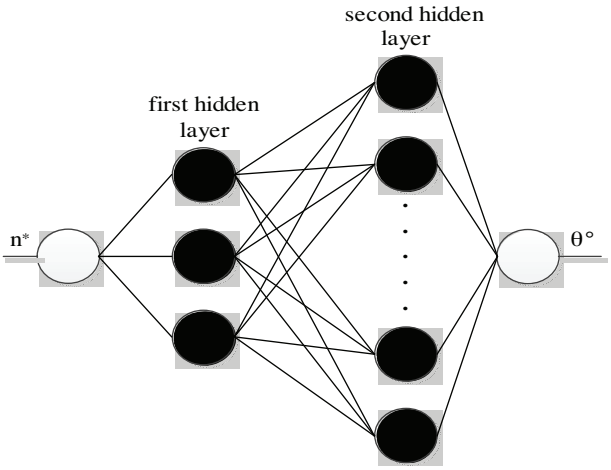

Figure 9. Structure of ANN.

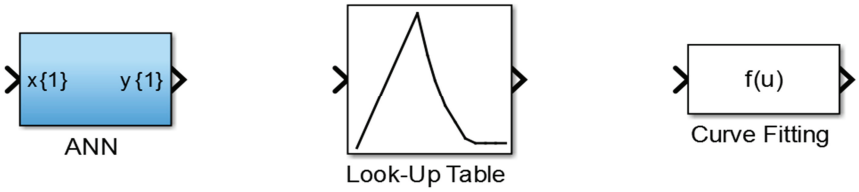

Figure 10. The MATLAB/Simulink blocks of the controllers.

The model shown in Figure 11 was developed to analyze the process performance of the controllers. By using the test data in Table 2, thyristor switching angles were determined according to wind speeds. Controllers in Figure 10 were separately used in the controller block shown in Figure 11, and the processing times were analyzed. The processing times of the simulations were determined by using the profiler in the MATLAB/Simulink tools. These results are provided in Table 3. As can be seen in Table 3, the ANN controller had 244.27% better process time performance than the LUT controller and 274.05% better process time performance than the CF controller. On the other hand, the LUT controller had 8.65% better process time performance than the CF controller.

Table 3. Process time performances of the controllers.

	ANN	LUT	CF
Process time (s)	2.0436131	7.0356451	7.644049

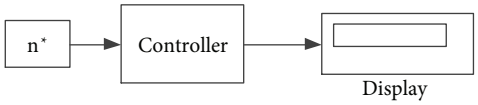

Figure 11. The model for the process time performance analysis of the controllers.

$p_1 = -1.207 \times 10^{-13}$

$p_2 = -2.262 \times 10^{-10}$

$p_3 = 9.332 \times 10^{-7}$

$p_4 = -0.000705$

$p_5 = 0.07281$
$p_6 = 49.61$

$$f(x) = p_1x^5 + p_2x^4 + p_3x^3 + p_4x^2 + p_5x + p_6 \tag{11}$$

7. Experimental results

According to the data in Table 1, which were used for testing the controllers, experimental results of the ANN, LUT, and CF controllers are shown in Table 4, Table 5, and Table 6, respectively. In addition, the variation of these results is shown in Figure 12, Figure 13, and Figure 14, respectively. Table 7 shows the percentage error ratio of the controllers related to the MPPT. According to the test data in Table 1, if Table 7 is analyzed, it is shown that the ANN controller gives the best MPPT results among them. In addition, an analysis of the performance of ANN, LUT, and CF controllers according to 20 different data demonstrated a decrease in error ratios of 51.43%, 50.18%, and 25.66%, respectively. According to the obtained results, increasing the data used for training the controllers will also increase their performance. In addition, it was also observed that increasing the training data for the ANN and LUT controllers led to a proportional increase in their performance. On the other hand, with the CF controller, 50% less improvement was observed in comparison to the other controllers.

Table 4. Test results for the ANN controller.

n^* (rpm)	Angle (θ °) predicted by the ANN	Obtained power P_{max} (W)
275	65	123.569
325	53	177.108
375	34	251.615
425	25	323.582
475	15	406.235
525	8	494.885
575	2	597.307
625	2	673.529
675	2	749.789
725	2	829.598

Table 5. Test results for the LUT controller.

n^* (rpm)	Angle (θ °) predicted by the ANN	Obtained power P_{max} (W)
275	55	105.891
325	51	180.107
375	36	250.352
425	25	323.582
475	15	406.235
525	8	494.885
575	4	591.554
625	2	673.529
675	2	749.789
725	2	829.598

The DC motor, PMSG, encoder, and control units represent a part of the set-up whose block diagram is shown in Figure 5. A picture of these units can be seen in Figure 15. Table 8 provides the PMSG parameters used in the experimental set. They were obtained as in [25].

Table 6. Test results for the CF controller.

n^* (rpm)	Angle (θ °) predicted by the ANN	Obtained power P_{max} (W)
275	70	85.384
325	51	180.107
375	36	250.352
425	23	298.498
475	15	406.235
525	8	494.885
575	2	597.307
625	0	666.452
675	0	741.316
725	2	829.598

Table 7. Controller performance in maximum power point tracking.

Controllers	Percentage error according to 10 test data	Percentage error according to total 20 test data
ANN	0.35	0.17
LUT	2.81	1.4
CF	8.34	6.2

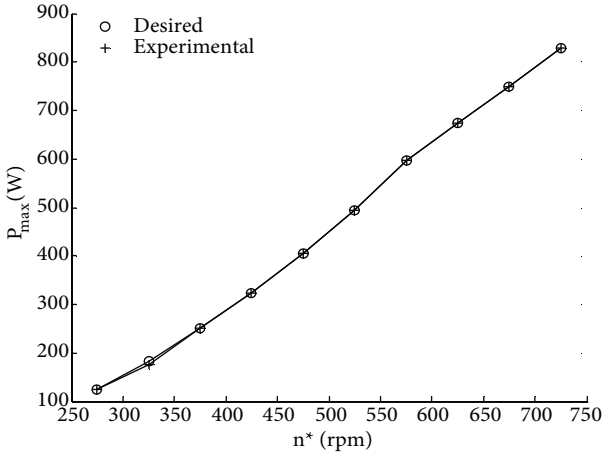

Figure 12. Changes in MPPT for the ANN controller.

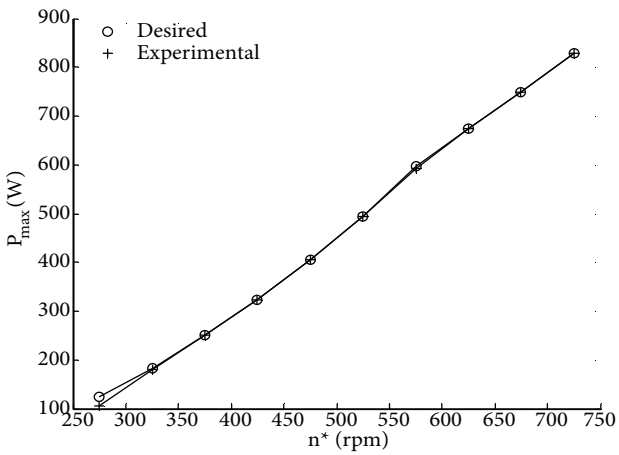

Figure 13. Changes in MPPT for the LUT controller.

Table 8. Parameters of the PMSG.

P (pairs of poles)	8
r_s (Ω)	1.35
L_q (mH)	5.893
L_d (mH)	7,967
λ_m (Wb)	0.3937
B (Nm/(rad/s))	1.25
J (kgm^2)	0.0095

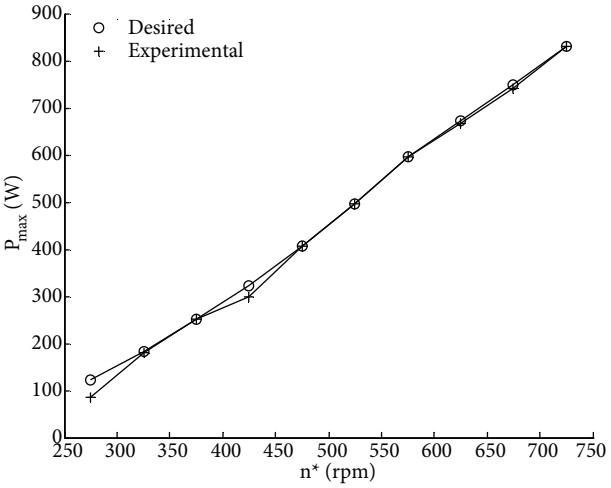

Figure 14. Changes in MPPT for the CF controller.

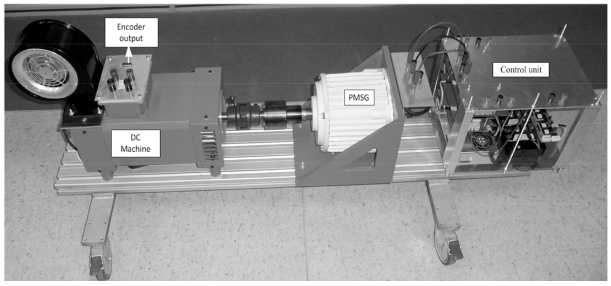

Figure 15. A part of the experimental set-up.

8. Conclusion

In this study, the MPPT and the process performance of the ANN, LUT, and CF controllers were determined based on experimental results. It was observed that the ANN, LUT, and CF controllers performed MPPT with 0.35%, 2.81%, and 8.34% error, respectively. In addition, it was determined that the ANN controller's performance was 244.27% better than that of the LUT controller and 274.05% better than that of the CF controller. On the other hand, the LUT controller's performance was 8.65% better than that of the CF controller. It was also determined that increasing the amount of data used in the training of the controllers would increase the performances of the ANN and LUT controllers, while the improvement observed with the CF controller in such a case would be approximately 50% less compared to the other controllers. In conclusion, the experimental results confirmed that the ANN controller was superior to the other controllers (the LUT and CF controllers) in terms of MPPT and process performance.

Acknowledgment

This work was supported by the Kocaeli University Scientific Research Project Center (Grant No. 2010/015).

References

[1] Hui Li, Shi KL, McLaren PG. Neural-network-based sensorless maximum wind energy capture with compensated power coefficient. IEEE T Ind Appl 2005; 41: 1548-1556.

[2] Eskander MN. Neural network controller for a permanent magnet generator applied in a wind energy conversion system. Renew Energ 2002; 26: 463-477.

[3] Bharanikumar R, Kumar AN. Performance analysis of wind turbine-driven permanent magnet generator with matrix converter. Turk J Electr Eng Co 2012; 20: 299-317.

[4] Lin CH. Recurrent wavelet neural network control of a PMSG system based on a PMSM wind turbine emulator. Turk J Electr Eng Co 2014; 22: 795-824.

[5] Demirtaş M, Şerefoğlu Ş. Design and implementation of a microcontroller-based wind energy conversion system. Turk J Electr Eng Co 2014; 22: 1582-1595.

[6] Meharrar A, Tioursi M, Hatti M, Stambouli AB. A variable speed wind generator maximum power tracking based on adaptative neuro-fuzzy inference system. Expert Syst Appl 2011; 38: 7659-7664.

[7] Zhang H, Xin X, Li L, Liu Q. Estimating global solar radiation using a hybrid parametric model from MODIS data over the Tibetan Plateau. Sol Energy 2015; 112: 373-382.

[8] Benammar M, Ben-brahim L, Alhamadi MA, Al-Naemi M. A novel method for estimating the angle from analog co-sinusoidal quadrature signals. Sensor Actuat-A Phys 2008; 142: 225-231.

[9] Pradhan R, Subudhi B. Design and real-time implementation of a new auto-tuned adaptive MPPT control for a photovoltaic system. Int J Elec Power 2015; 64: 792-803.

[10] Garrigos A, Blanes JM, Carrasco JA, Ejea JB. Real time estimation of photovoltaic modules characteristics and its application to maximum power point operation. Renew Energ 2007; 32: 1059-1076.

[11] Krishnan R, Rim GH. Performance and design of a variable speed constant frequency power conversion scheme with a permanent magnet synchronous generator. In: Industry Applications Society Annual Meeting; 1–5 October 1989; San Diego, CA, USA. pp. 45-50.

[12] Mengi OÖ, Altaş İH. Fuzzy logic control for a wind/battery renewable energy production system. Turk J Electr Eng Co 2012; 20: 187-206.

[13] Benchagra M, Maaroufi M, Ouassaid M. A performance comparison of linear and nonlinear control of a SCIG-wind farm connecting to a distribution network. Turk J Electr Eng Co 2014; 22: 1-11.

[14] Schiemenz I, Stiebler M. Control of a permanent magnet synchronous generator used in a variable speed wind energy system. In: Electric Machines and Drives Conference; 17–20 June 2001; Cambridge, MA, USA. pp. 872-877.

[15] Amei K, Takayasu Y, Ohji T, Sakui M. A maximum power control of wind generator system using a permanent magnet synchronous generator and a boost chopper circuit. In: Power Conversion Conference; 2–5 April 2002; Osaka, Japan. pp. 1447-1452.

[16] Senjyu T, Tamaki S, Urasaki N, Uezato K, Funabashi T, Fujita H. Wind velocity and position sensorless operation for PMSG wind generator. In: The Fifth International Conference on Power Electronics and Drive Systems; 17–20 November 2003; Singapore. pp. 787-792.

[17] Matsui M, Dehong X, Longyun K, Yang Z. Limit cycle based simple MPPT control scheme for a small sized wind turbine generator system-principle and experimental verification. In: Power Electronics and Motion Control Conference; 14–16 August 2004; Xi'an, China. pp. 1746-1750.

[18] Dai J, Xu D, Wu B. A novel control system for current source converter based variable speed PM wind power generators. In: Power Electronics Specialists Conference; 17–21 June 2007; Orlando, FL, USA. pp. 1852-1857.

[19] Nishida K, Ahmed T, Nakaoka M. A cost-effective high-efficiency power conditioner with simple MPPT control algorithm for wind-power grid integration. IEEE T Ind Appl 2011; 47: 893-900.

[20] Xu Z, Li R, Zhu H, Xu D, Zhang CH. Control of parallel multiple converters for direct-drive permanent-magnet wind power generation systems. IEEE T Power Electr 2012; 27: 1259-1270.

[21] Barote L, Marinescu C, Cirstea MN. Control structure for single-phase stand-alone wind-based energy sources. IEEE T Ind Electron 2013; 60: 764-772.

[22] Chinchilla M, Arnaltes S, Burgos JC. Control of permanent-magnet generators applied to variable-speed wind-energy systems connected to the grid. IEEE T Energy Conver 2006; 21: 130-135.

[23] Westlake AJG, Bumby JR, Spooner E. Damping the power-angle oscillations of a permanent-magnet synchronous generator with particular reference to wind turbine applications. IEEE P-Elect Pow Appl 1996; 143: 269-280.

[24] Dai J, Xu D, Wu B. A novel control scheme for current-source-converter-based PMSG wind energy conversion systems. IEEE T Power Electr 2009; 24: 963-972.

[25] Karakaya A, Karakas E. Performance analysis of PM synchronous motors using fuzzy logic and self tuning fuzzy PI speed controls. Arab J Sci Eng 2008; 33: 153-177.